EAST EUROPEAN JOURNAL OF PHYSICS. **2.** 292-301 (2026)
DOI:10.26565/2312-4334-2026-2-31 ISSN 2312-4334

A NUMERICAL SIMULATION STUDY INVESTIGATING THE FUNCTIONALITY OF A PEROVSKITE SOLAR CELL BASED ON $FASnI_3$ IN BOTH CONVENTIONAL AND INVERTED CONFIGURATIONS USING COMPATIBLE $Zn(O_{0.3}S_{0.7})$ AS THE ELECTRON TRANSPORT LAYER

M.V. Kavitha[1,2], K.S. Sudheer[1,3]***
[1]*Opto-electronic Device Simulation Research Lab, Department of Physics, Christ College (Autonomous), Irinjalakuda, University of Calicut, Kerala, India, PIN-680125*
[2]*Department of Physics, Sree Narayana College, Nattika, University of Calicut, Kerala, India, PIN-680566*
[3]*Department of Physics, St. Aloysius College, Thrissur, University of Calicut, Kerala, India, PIN-680611*
**Corresponding Author email: sudheersebastian@christcollegeijk.edu.in; **e-mail: kavitha.9667@christci.in*
Received February 1, 2026; revised April 22, 2026; accepted April 24, 2026

Formamidinium Tin Iodide is a promising candidate as an absorber layer in perovskite solar cells due to its tunable bandgap, high absorption coefficient, and good thermal stability. The selection of suitable charge transport layers with the proper band offset can effectively reduce recombination at interfaces and improve solar cell performance. The study focuses on enhancing the performance of a perovskite solar cell in which Formamidinium Tin Iodide ($FASnI_3$) is the absorber layer, $Zn(O_{0.3}S_{0.7})$ is the ETL and Spiro-OMeTAD is the HTL using numeric simulation. These charge-transport-layer materials are selected based on their adequate energy band alignment with the absorber. The structure Glass substrate/FTO/$Zn(O_{0.3}S_{0.7})$(ETL)/$FASnI_3$/Spiro-OMeTAD(HTL)/Au, which is an unexplored combination in n-i-p architecture, is simulated through SCAPS-1D and optimization of cell parameters- absorber thickness, absorber doping concentration, absorber defect density, ETL thickness, ETL defect density, HTL thickness, and HTL defect density- is carried out. The variation of cell performance parameters with interface defect density and temperature is also analyzed. With this optimization, the cell delivers an open circuit voltage (V_{oc}) = 1.0145V, short circuit current density (J_{sc}) = 37.82mA cm^{-2}, fill factor (FF) = 83.31% and Power Conversion Efficiency (PCE) =31.97%. The optimized parameters are used to simulate the p-i-n inverted architecture, and the cell output is as follows.V_{oc} = 1.0919V, J_{sc} = 37.293mA cm^{-2}, FF = 83.01% and Power Conversion Efficiency(PCE) =33.8%.
Keywords: *Perovskite solar cell; SCAPS; Formamidinium Tin Iodide; Spiro-OMeTAD, ZnOS*
PACS: 02.60.Cb, 61.72.-y, 42.79.Ek, 84.60.Jt

1. INTRODUCTION

In the realm of renewable energy, perovskite solar cells have demonstrated immense potential, with efficiency increasing exponentially over the past decade. Their unique opto-electronic properties, excellent absorptivity, simple and low-cost preparation and processing, etc., made them inevitable in the field of photovoltaics [1–3]. Organic and inorganic Lead halide perovskite are highly efficient candidates among perovskite solar cells. Even though Lead-based perovskite solar cells reported a breakthrough advancement in efficiency of 25.7%[4–6], their toxicity hinders large-scale commercialization.

Among the Tin-based perovskite solar cells, $FASnI_3$ possesses an appropriate bandgap (1.41 eV) and high mobility, which are desirable for solar cell applications. The oxidation of Sn^{2+} into $Sn^{4+}$is the major stability problem associated with $FASnI_3$.This increases the p-type conductivity of the material and results in low value of efficiency[7,8]. The incorporation of organic additives can enhance the efficiency and act as passivating agents of defects in $FASnI_3$[9,10]. The addition of SnF_2 is also an efficient method to tackle the problem of Sn^{2+} oxidation in $FASnI_3$[11].The $FASnI_3$ layer fabricated with vertical Sn^{2+} gradient using Lewis base-assisted recrystallization method showed an efficiency of 13.82%[12].

Electron Transport Layer (ETL) and the Hole Transport Layer (HTL) are essential for the extraction and collection of photogenerated electrons and holes produced inside the absorber layer in a solar cell structure. Effective charge transport is the primary factor determining the efficiency of a solar cell. The band offset at the interface of the absorber and charge transport layer plays a crucial role in the extraction of charge carriers[13]. The device modelling and optimization of perovskite solar cell with $FASnI_3$ as absorber material, Spiro-OMeTAD as Hole Transport Layer (HTL) and $Zn(O_{0.3}S_{0.7})$ as Electron Transport Layer forms the basis of the current work. $Zn(O_{0.3}S_{0.7})$ is a worthy candidate as an ETL in perovskite solar cells. It provides a suitable band alignment with FASnI3, thereby reducing charge recombination at the interface. Since $Zn(O_{0.3}S_{0.7})$ has significantly greater electron mobility than the commonly used ETL TiO_2, electrons can be extracted from the perovskite absorber layer more quickly and effectively. This improves current density (J_{sc}) and power conversion efficiency (PCE) by lowering charge accumulation and recombination losses[14]. By reducing interfacial trap states and suppressing charge recombination, a well-matched ETL like $Zn(O_{0.3}S_{0.7})$ can indirectly passivate the perovskite surface defects[15]. $Zn(O_{0.3}S_{0.7})$ as ETL can restrict the amount of oxygen and moisture that can enter from the top contact of the cell and lessen the possibility of Sn oxidation at the interface and improves the chemical stability of the underlying $FASnI_3$[15]. Ayush Tara et al. simulated the structure FTO/$Zn(O_{0.3}S_{0.7})$/$FASnI_3$/CuSCN/Au and attained

Cite as: M.V. Kavitha, K.S. Sudheer, East Eur. J. Phys. 2, 292 (2026), https://doi.org/10.26565/2312-4334-2026-2-31

an efficiency of 25.94%[16]. Au/NiO/$FASnI_3$/$ZnO_{0.25}S_{0.75}$/FTO is simulated by Srinivas Mattaparthi et al. and an efficiency of around 31.57% is obtained[17].

The PV community is searching for hole transport materials that are inexpensive, provide high charge carrier mobility, and stability. Both organic and inorganic materials can be used as HTLs. Even though inorganic materials are abundant, low-cost and stable, they are still behind organic HTLs from the efficiency point of view[18]. For the effective extraction of the carriers, the Highest Occupied Molecular Orbital (HOMO) of HTL should be placed above the HOMO level of absorber and Lowest Unoccupied Molecular Orbital (LUMO)level of ETL should be placed below the absorber LUMO level. The chosen HTL spiro-OMeTAD satisfies this condition. The additive engineering can greatly improve the stability of spiro-OMetAD, which is a major challenge faced by researchers. Also, photo-accelerated oxidation of Spiro-OMeTAD is an efficient and rapid process for the manufacturing and industrial applications of Spiro-OMeTAD[19]. The impact of absorber layer thickness, doping concentration, defect density, ETL thickness, doping concentration, HTL thickness, doping concentration, interface defect density and temperature, on the cell performance parameters is discussed in detail and performance optimization is done in this work.

2. METHODOLOGY AND DEVICE MODELLING

The device simulation and optimization of the structure Glass substrate /FTO/$Zn(O_{0.3}S_{0.7})$(ETL)/$FASnI_3$/Spiro-OMeTAD(HTL)/Au is done with Solar Cell Capacitance Simulator software. A lot of research is being done with this computational software and it is based on solving the Poisson's equation and continuity equations for the charge carriers

$$\frac{\partial}{\partial x}\varepsilon_0\varepsilon\frac{\partial\psi}{\partial x} = -q\left(p - n + N_D - N_A + \frac{\rho_{def}}{q}\right) \quad (1)$$

$$\frac{\partial n}{\partial t} = -\frac{\partial J_n}{\partial x} - U_n + G \quad (2)$$

$$\frac{\partial p}{\partial t} = -\frac{\partial J_p}{\partial x} - U_p + G \quad (3)$$

$$J_n = -\mu_n n q\frac{\partial E_{Fn}}{\partial x} \quad (4)$$

$$J_p = +u_p p q\frac{\partial E_{Fp}}{\partial x} \quad (5)$$

ε stands for the permittivity, ε_0 for the free space permittivity, ψ for the electrostatic potential, and q for the charge. n and p represent the concentration of electrons and holes, whereas N_D and N_A denote the ionized donor and ionized acceptor doping concentrations. ρ_{def} stands for defect distribution, whereas J_n and J_p stand for electron and hole current densities. U_n represents the electron recombination rate, U_p the hole recombination rate, G stands for the generation rate of carriers. Electron and hole mobilities are represented by μ_n and μ_p. E_{Fn} and E_{Fp} represent the electron and hole quasi-Fermi levels[20].

The standardization of the software is done by comparing the simulation results of the structure Glass substrate/FTO/TiO_2(ETL)/$FASnI_3$/Spiro-OMeTAD(HTL)/Au with the experimental data [8,20,21] in our previous work. Figure 1 shows the schematic representation of the structure being studied. Figure 2 shows the HOMO and LUMO levels of the layers. While the LUMO level of $Zn(O_{0.3}S_{0.7})$ is below $FASnI_3$, the HOMO level of Spiro-OMeTAD is in the same level as $FASnI_3$. The offset of valence band (VBO) at the Spiro-OMeTAD/$FASnI_3$ interface is zero and the offset of conduction band (CBO) at this interface is -1.47eV. The CBO at the $FASnI_3$/$Zn(O_{0.3}S_{0.7})$ interface is 0.08 eV and the VBO at this interface is -1.5 eV. For the efficient charge carrier extraction and collection, a small value of VBO and a large value of CBO are preferable at the Spiro-OMeTAD/$FASnI_3$ interface. Also small value of CBO and a large value of VBO are preferable at the $FASnI_3$/$Zn(O_{0.3}S_{0.7})$interface[20].

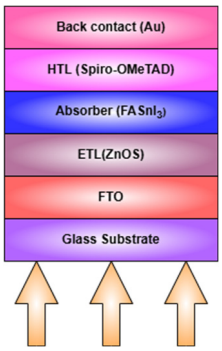

Figure 1. Device configuration

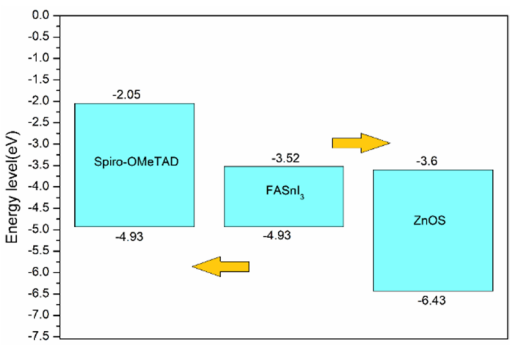

Figure 2. HOMO and LUMO levels of absorber, ETL and HTL

The required simulation parameters are obtained from the published literature. Table 1 lists the parameters needed for simulation. The electron and hole thermal velocities are fixed at 10^7cm/s. The defect density at the Spiro-

OMeTAD/$FASnI_3$ as well as at the $FASnI_3$/$Zn(O_{0.3}S_{0.7})$ interface is set at 10^{16} cm^{-3}. The simulation is performed at an operating temperature of 300K under an illumination of AM1.5G spectrum with an intensity of 1000 mW/cm^2.

Table 1. Simulation parameters of each layer

Parameters	FTO	$Zn(O_{0.3}S_{0.7})$	$FASnI_3$	Spiro-OMeTAD
Thickness (nm)	500[8]	30	350[21]	200[22]
Band gap ,E_g(eV)	3.5[8]	283[16]	1.41[21]	2.88[22]
e-affinity (eV)	4[8]	3.6[16]	3.52[23]	2.05[22]
Dielectric Permittivity, ε_r	9[8]	9[16]	8.2[23]	3[22]
Effective density of states at CB(cm^{-3})	2.2×10^{18}[8]	2.2×10^{18}[22]	1.0×10^{18}[23]	2.2×10^{18}[22]
Effective density of states at VB (cm^{-3})	1.8×10^{19}[8]	1.8×10^{19}[22]	1.0×10^{19}[23]	1.8×10^{19}[22]
e−mobility μ_n,($cm^2V^{-1}S^{-1}$)	20[8]	100	22[23]	2.0×10^{-4}[22]
h^+mobility μ_p, ($cm^2V^{-1}S^{-1}$)	10[8]	25	22[23]	2.0×10^{-4}[22]
Donor density N_D (cm^{-3})	2.0×10^{19}[8]	9.0×10^{16}	-	-
Acceptor density N_A (cm^{-3})	-	-	7.0×10^{16}[23]	2.0×10^{19}[22]
Density of defects, N_t (cm^{-3})	1.0×10^{15}[8]	1.0×10^{15}[13]	2.0×10^{15}[23]	1.0×10^{15}[22]

Figure 3 depicts the structure's energy band diagram. Since Spiro-OMeTAD and $Zn(O_{0.3}S_{0.7})$ provide adequate band offset at the interface of $FASnI_3$, there are no cliffs or peaks found at the interface. The performance parameters- Open circuit Voltage(V_{oc}), short circuit current density (J_{sc}), fill factor (FF) and power conversion efficiency (PCE) -of the device on initial simulation are summarized in Table 2. Figure 4 shows the variation of quantum efficiency with wavelength of radiation. The quantum efficiency curve spans the whole visible spectrum and shows maximum efficiency at 500nm. The cell performance parameters on the initial simulation are listed in Table 2. The variation of cell performance parameters with respect to thickness of absorber, defect density of absorber, doping concentration of absorber, defect density of ETL, thickness of ETL, defect density of HTL, thickness of HTL, defect density at the HTL/absorber interface, defect density at the absorber/ETL interface and temperature etc are analyzed in the next section.

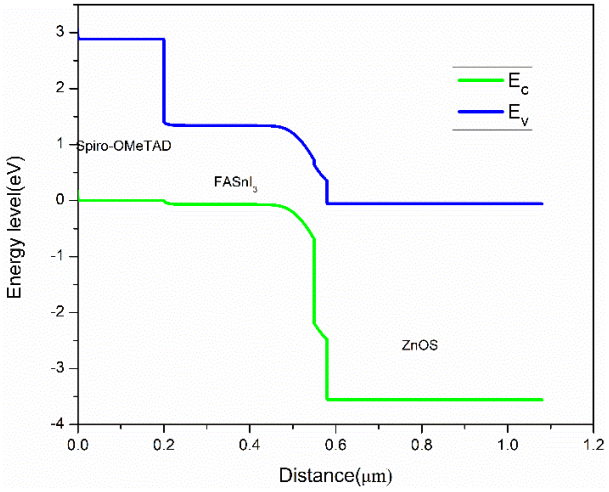

Figure 3. Energy band diagram

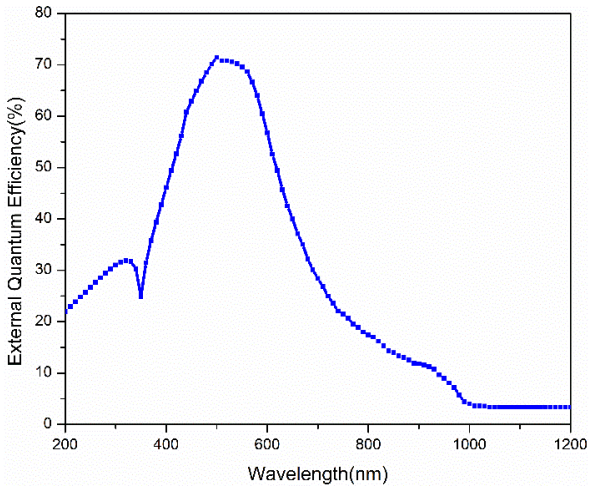

Figure 4. Quantum efficiency curve

Table 2. Initial performance parameters of the cell

V_{oc}(V)	J_{sc}(mA/cm^2)	FF(%)	PCE(%)
0.3464	14.797194	49.35	2.53

3. RESULTS AND DISCUSSION

3.1 Influence of Varying Absorber Layer Thickness

The variation of cell performance parameters with thickness is depicted in Figure 5. Power conversion efficiency increases with thickness from 0 to 1 µm, peaks at 3.26% at 0.75 µm, and then decreases. An increase in thickness leads to greater photon absorption, thereby improving efficiency. However, after saturation, efficiency diminishes because charge carriers may not reach the appropriate electrodes, as the thickness is considerably greater than the diffusion length [4]. J_{sc} also shows the same behaviour. V_{oc} decreases first, becomes constant over a range and slightly decreases after 0.75µm. This could be due to the increase in recombination rate. Fill factor decreases first due to the increase in series resistance [22], becomes constant and increases after 0.75µm. This is because of the decrease in V_{oc} and J_{sc}at this value of thickness.

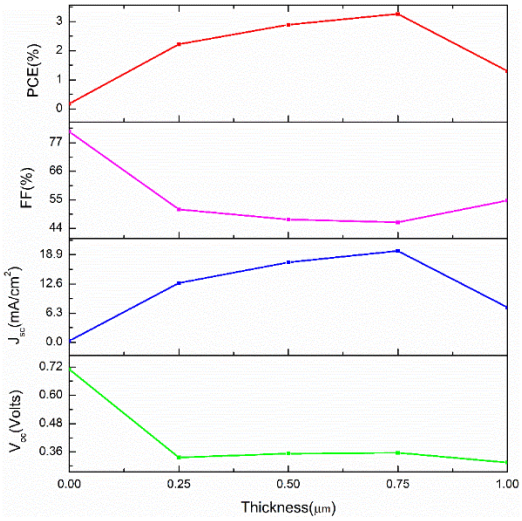

Figure 5. Effect of varying absorber thickness on performance parameters

3.2 INFLUENCE OF VARYING ABSORBER LAYER DEFECT DENSITY

The creation of processing sequences that can reduce harmful impurities, point and cluster defects, is the key task in the production of solar cells. A lot of methods are introduced for passivating unavoidable defects. The defects act as trap states, which can lead to non-radiative SRH recombination[24,25]. Here we study the variation of performance parameters with varying defect density from 10^{14} to 10^{18} cm^{-3}. The results are portrayed in Figure 6. As the defect density increases, the V_{oc}, J_{sc} and efficiency decrease. Fill factor slightly rises first, but this is compensated by the decrease in V_{oc} and J_{sc} and thereby reducing the value of PCE. The defect density and the diffusion length of the carriers are related by the equation

$$L = \sqrt{D\tau} \tag{6}$$

L stands for the diffusion length, D for the diffusion coefficient and τ for the carrier lifetime.

The equation for the diffusion coefficient is

$$D = \frac{\mu k_B T}{q} \tag{7}$$

μ stands for charge carrier mobility, K_B for the Boltzmann constant, T for the temperature and q for the charge

Relaxation time of carriers is given by the equation

$$\tau = \frac{1}{\sigma N_t V_{th}} \tag{8}$$

σ stands for the capture cross-section of carriers, N_t for the defect density and V_{th} for the thermal velocity of carriers. Figure 7 shows the variation of the generation rate of carriers with depth at different defect densities. It is seen that the generation rate is the same for all defect densities. Figure 8 shows the variation of the recombination rate of carriers with depth at different defect densities. As the defect density rises, so does the recombination rate. Since it offers the highest efficiency of 2.59%, 10^{14} cm^{-3} is selected as the optimum value of defect density. Also, it provides a diffusion length of 1.687μm and the chosen thickness lies within this limit of diffusion length.

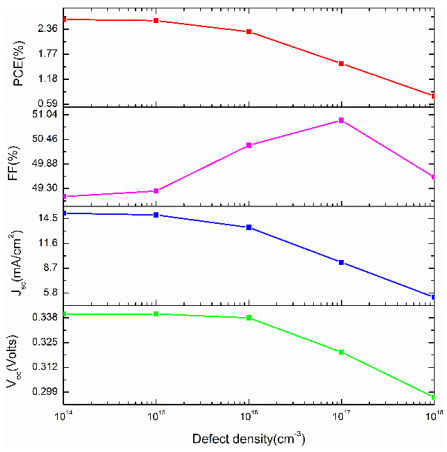

Figure 6. Effect of varying defect density on performance parameter

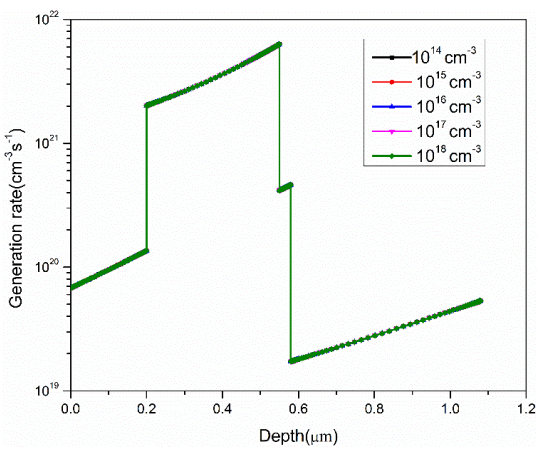

Figure 7. Variation of generation rate with depth at different defect densities

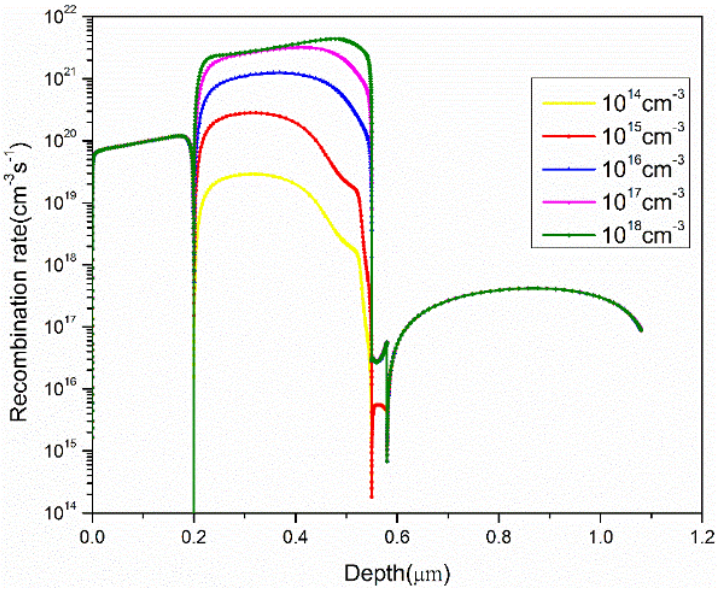

Figure 8. Variation of recombination rate with depth at different defect densities

3.3 INFLUENCE OF VARYING ABSORBER LAYER DOPING CONCENTRATION

The absorber material is a p-type semiconductor and the doping concentration represents the concentration of holes. Generally, increasing the doping level improves the conductivity of the material and hence, the performance parameters increase. Here, the doping concentration is varied from 10^{13} to 10^{17} cm^{-3} and Figure 9 shows the variation of cell performance parameters. The performance parameters remain almost constant with a rise in doping concentration up to 10^{15} cm^{-3} and then decrease. The initial doping concentration is 7×10^{16} cm^{-3}. The doping has a great impact on the cell performance. On reducing the doping concentration to 10^{13} cm^{-3}, the efficiency increases to 8.18%. The decrease in performance at high doping concentration can be attributed to the increase in Auger recombination [26–28].

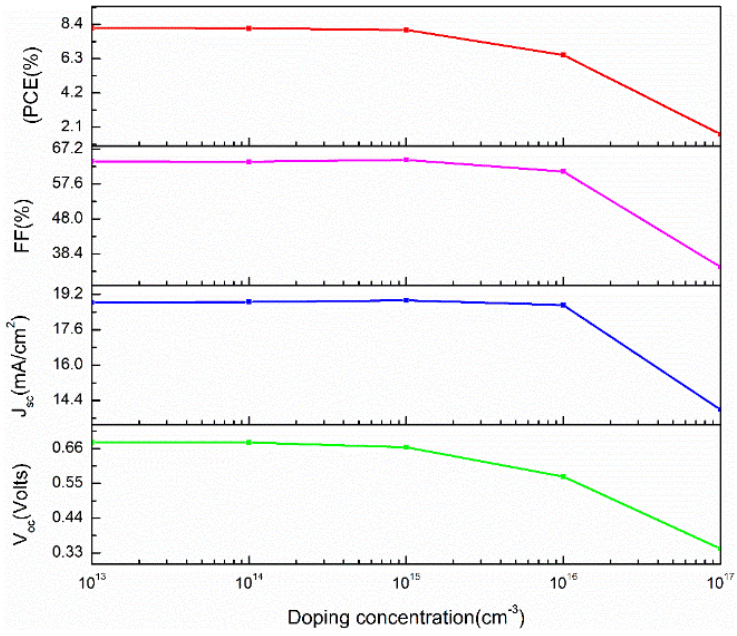

Figure 9. Effect of varying doping concentration on performance parameters

3.4 INFLUENCE OF VARYING ETL AND HTL THICKNESS

The thickness of ETL is varied from 20 to 50nm, whereas the thickness of HTL is varied from 100 to 500nm. The performance parameters obtained are depicted in Figure 10. The figure shows that the HTL thickness does not have much influence on the performance parameters. So, it is optimized at a minimum thickness of 100nm. As the ETL thickness increases, the performance parameters decrease. The efficiency is maximum (3.17%) at an ETL thickness of 20nm. The decrease in efficiency is attributed to the partial absorption of photons by ETL at high thickness[20,29].So the optimum ETL thickness is selected as 20nm.

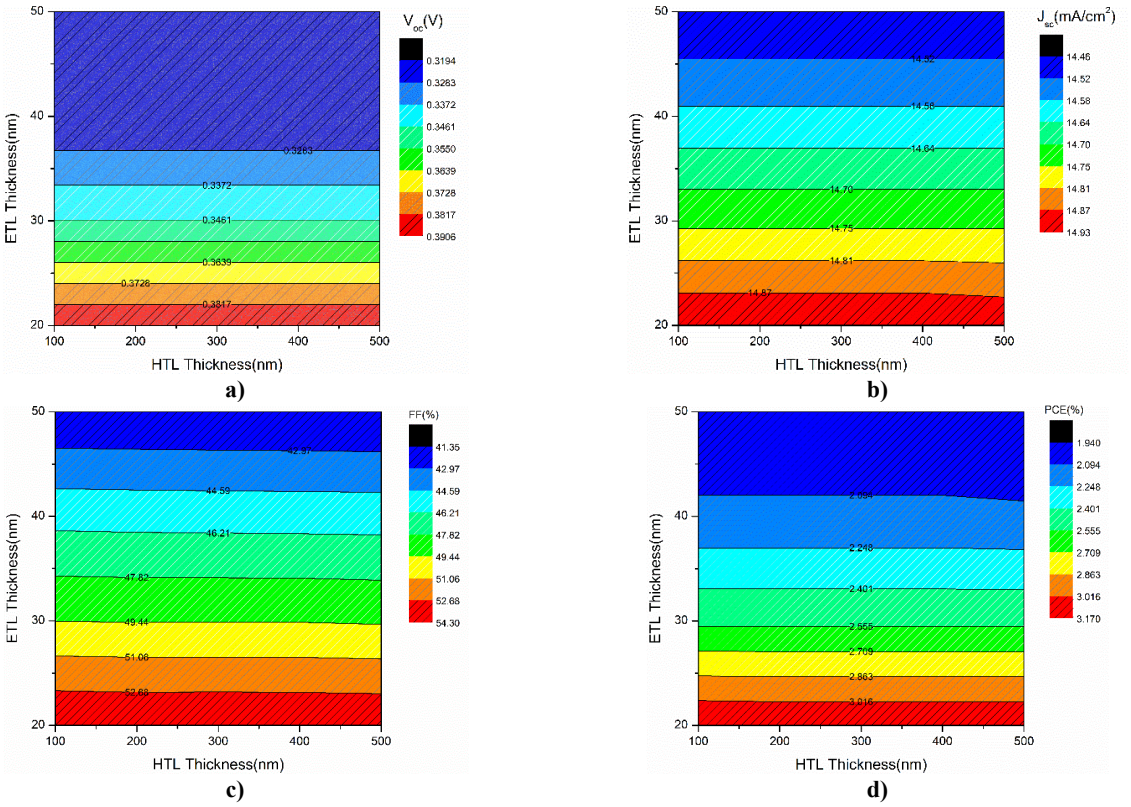

Figure 10. Effect of varying ETL and HTL thickness on a) V_{oc}; b) J_{sc}; c) FF; d) PCE

3.5 INFLUENCE OF VARYING ETL AND HTL DOPING CONCENTRATION

ETL and HTL are necessary for the extraction and transport of charge carriers to the respective electrodes. The increase in doping concentration of ETL and HTL improves the performance parameters. This is because of the increase in the electric field at the interface[30,31].The results of varying doping concentration on the performance parameters are portrayed in Figure 11.

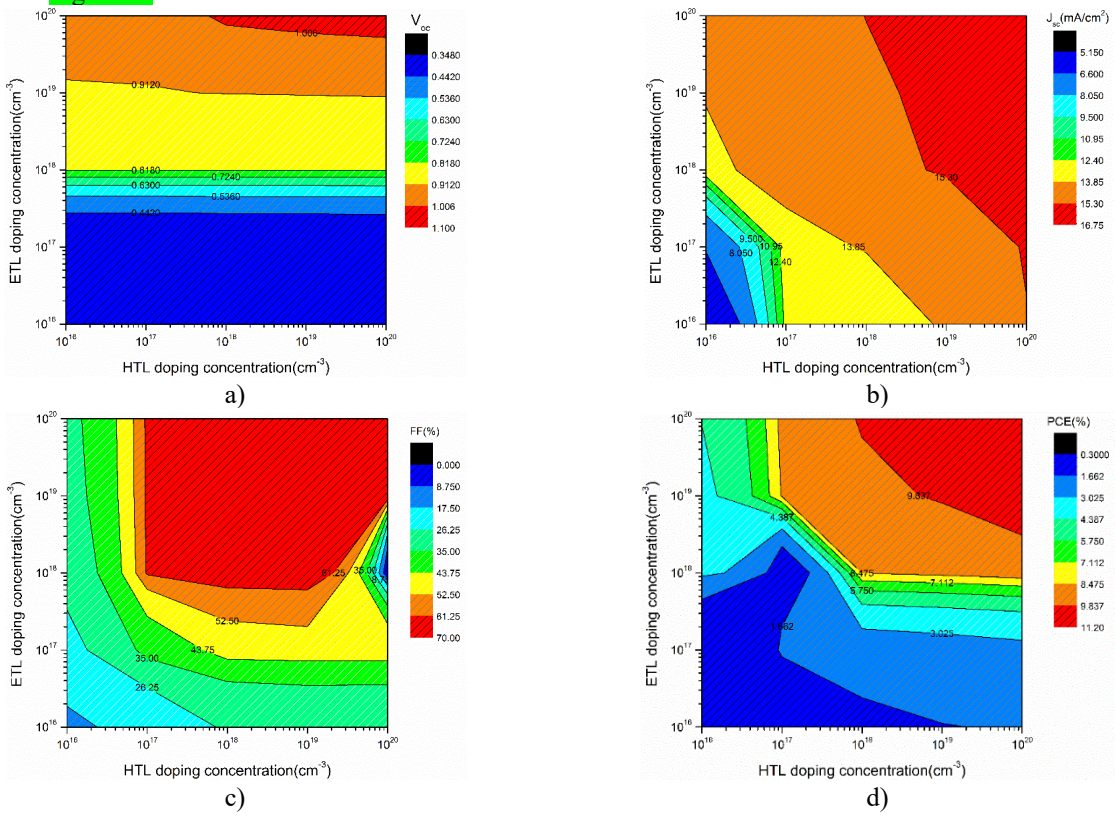

Figure 11. Effect of varying ETL and HTL doping concentration on a) V_{oc}; b) J_{sc}; c) FF; d) PCE

Both the ETL and HTL doping concentrations are varied from 10^{16} to 10^{20} cm^{-3}. All the performance parameters increase with the ETL and HTL doping concentration. The performance parameters yield the maximum value at a doping concentration of 10^{20} cm^{-3} for both the transport layers. The efficiency reaches a maximum value of 11.2% at this doping concentration.

3.6 INFLUENCE OF VARYING INTERFACE DEFECT DENSITY AT THE HTL/ABSORBER INTERFACE AND ETL/ABSORBER INTERFACE

The defect density at both the HTL/absorber and ETL/absorber interface is varied from 10^{10} to 10^{17} cm^{-3}. The variation of performance parameters is depicted in Figure 12 and Figure 13. The defects at the interfaces are common because it is the junction between two structurally different layers. As the interface defect density increases, the performance parameters decrease. The efficiency varies from 3.09 to 2.52% with the variation of HTL/absorber defect density. The efficiency varies from 10.57 to 2.52% with the variation of ETL/absorber defect density. The ETL/absorber interface defect density has a much higher impact on performance parameters. At the interfaces, minority charge carrier recombination occurs and the recombination rate increases with an increase in interface defect density. So, interface modification to control the defect density is very essential in the fabrication of highly efficient perovskite solar cells[32,33].The optimum value of defect density is chosen as 10^{10} cm^{-3} at both the interfaces.

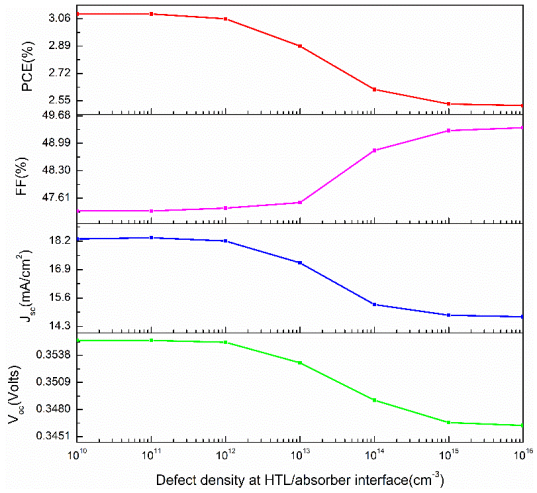

Figure 12. Effect of varying HTL/absorber interface defect density on the performance parameters

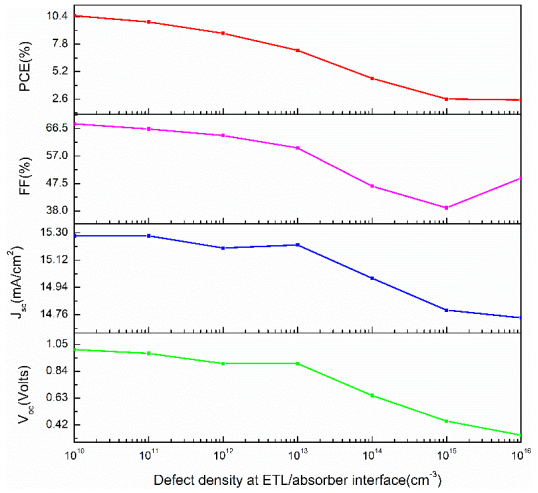

Figure 13. Effect of varying ETL/absorber interface defect density on the performance parameters

3.7 INFLUENCE OF VARYING TEMPERATURE

Figure 14 shows how the performance parameters vary with the operating temperature. The range of temperature variation is from 280K to 320K. As the temperature increases, the performance parameters decrease. V_{oc} varies from 0.39 to 0.30V. J_{sc} slightly decreases from 14.74 to 14.71mA/cm^2. The Fill factor decreases from 52.07 to 45.54% and the efficiency decreases from 3.06 to 2.01%. The increase in series resistance owing to the increased recombination rate accounts for the observed behaviour of performance parameters[20,34,35].

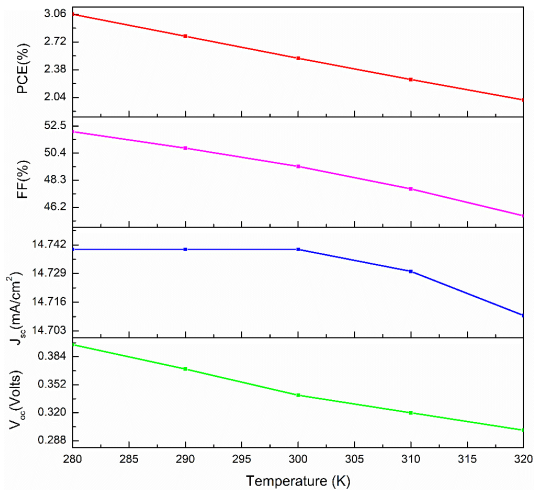

Figure 14. Effect of varying temperature on the performance parameters

The simulation is again performed with the optimized parameters such as absorber thickness of 750nm, absorber defect density of $10^{14}cm^{-3}$, absorber doping concentration of $10^{14}cm^{-3}$, ETL thickness of 20nm, ETL doping concentration of $10^{20}cm^{-3}$, HTL thickness of 100nm, HTL doping concentration of $10^{20}cm^{-3}$, interface defect density of $10^{10}cm^{-3}$ at both ETL/absorber interface and HTL/absorber interface and a temperature of 300K. The performance parameters obtained after optimization are listed in Table 3. All the cell performance parameters show a high improvement on optimization. The cumulative effect of all optimized parameters improves the efficiency to 31.97%.

Table 3. Cell performance parameters after optimization

V_{oc} (V)	J_{sc} (mA/cm^2)	FF(%)	PCE(%)
1.0145	37.824196	83.31	31.97

3.8 THE INVERTED (p-i-n) STRUCTURE

The optimized parameters are used to investigate the inverted (p-i-n) architecture of the solar cell, in which ETL replaces HTL and vice versa. The simulation of the architecture glass substrate/FTO/Spiro-OMeTAD(HTL)/$FASnI_3$/$Zn(O_{0.3}S_{0.7})$(ETL)/Au is executed, and the performance parameters obtained are listed in Table 4. The inverted structure offers better power conversion efficiency, and this could be due to the better material compatibility.

Table 4. Cell performance parameters of the inverted structure

V_{oc} (V)	J_{sc} (mA/cm^2)	FF(%)	PCE(%)
1.0919	37.29378	83.01	33.8

4. CONCLUSIONS

In this work, the eco-friendly solar cell n-i-p architecture, Glass substrate/FTO/$Zn(O_{0.3}S_{0.7})$(ETL)/$FASnI_3$/Spiro-OMeTAD(HTL)/Au, is simulated using SCAPS-1D software. The impact of cell parameters, including absorber thickness, absorber doping concentration, absorber defect density, ETL thickness, ETL defect density, HTL thickness, HTL defect density, interface defect density, and temperature, on cell performance is investigated. The optimized values of each of these cell parameters have been determined. The optimization resulted in an improved performance with V_{oc} of 1.0145 V, J_{sc} of 37.82mAcm^{-2}, fill factor of 83.31% and PCE of 31.97%. The inverted structure yielded a V_{oc} of 1.0919 V, J_{sc} of 37.293mA cm^{-2}, fill factor of 83.01%, and PCE of 33.8%. The greatest impact on efficiency is achieved by optimizing the absorber doping concentration. ETL doping concentration and interface defect density at the ETL/absorber interface also contribute much to the efficiency. So, careful optimization of cell parameters can significantly improve the performance. The proposed structure is a great option for experimental exploration and can be implemented with minimal performance compromise.

Data availability statement
The data that support the findings of this study are available from the corresponding author upon reasonable request.

Funding
This research did not receive any specific grant from funding agencies in the public, commercial, or not-for-profit sectors.

Acknowledgments
The authors would like to thank Marc Burgelman, Department of Electronics and Information Systems at the University of Gent, Belgium, for providing SCAPS software.

Conflict of interest
The authors declare no conflict of interest.

ORCID
Kavitha M.V., https://orcid.org/0009-0005-8611-6091; **Sudheer Sebastian K.,** https://orcid.org/0000-0002-9019-4405

REFERENCES

[1] S. Imani, S.M. Seyed-Talebi, J. Beheshtian, E.W.G. Diau, "Simulation and characterization of CH3NH3SnI3-based perovskite solar cells with different Cu-based hole transporting layers," Applied Physics A, **129**, 143 (2023). https://doi.org/10.1007/s00339-023-06428-0

[2] T. Wu, Z. Qin, Y. Wang, Y. Wu, W. Chen, S. Zhang, M. Cai, *et al.*, "The Main Progress of Perovskite Solar Cells in 2020–2021," Nanomicro Lett. **13**, (2021). https://doi.org/10.1007/s40820-021-00672-w

[3] J.Y. Kim, J.W. Lee, H.S. Jung, H. Shin, and N.G. Park, "High-Efficiency Perovskite Solar Cells," Chem. Rev. **120**, 7867–7918 (2020). https://doi.org/10.1021/acs.chemrev.0c00107

[4] M. Ismail, M. Noman, S. Tariq Jan, and M. Imran, "Boosting efficiency of eco-friendly perovskite solar cell through optimization of novel charge transport layers," R. Soc. Open. Sci. **10**, (2023). https://doi.org/10.1098/rsos.230331

[5] L. Lin, L. Jiang, P. Li, B. Fan, Y. Qiu, and F. Yan, "Simulation of optimum band structure of HTM-free perovskite solar cells based on ZnO electron transporting layer," Mater. Sci. Semicond. Process. (2019). https://doi.org/10.1016/j.mssp.2018.10.003

[6] M.V. Kavitha, C.K. Anjali, and K.S. Sudheer, "Device simulation and optimization of HTL-free perovskite solar cell with CH3NH3SnBr3 as the absorber layer using solar cell capacitance simulator software," Journal of Ovonic Research, **20**, 245–254 (2024). https://doi.org/10.15251/JOR.2024.202.245

[7] X. Meng, T. Wu, X. Liu, X. He, T. Noda, Y. Wang, H. Segawa, and L. Han, "Highly Reproducible and Efficient $FASnI_3$ Perovskite Solar Cells Fabricated with Volatilizable Reducing Solvent," J. Phys. Chem. Lett. **11**, 2965–2971 (2020). https://doi.org/10.1021/acs.jpclett.0c00923

[8] S. Abdelaziz, A. Zekry, A. Shaker, M. Abouelatta, Investigating the performance of formamidinium tin-based perovskite solar cell by SCAPS device simulation, Opt Mater (Amst) 101 (2020). https://doi.org/10.1016/j.optmat.2020.109738

[9] S. Galve-Lahoz, J. Sánchez-Diaz, C. Echeverría-Arrondo, J. Simancas, J. Rodriguez-Pereira, S.-H. Turren-Cruz, J.P. Martinez-Pastor, *et al*., "Addressing ambient stability challenges in pure $FASnI_3$ perovskite solar cells through organic additive engineering," J. Mater. Chem. A Mater. **12**, 21933–21943 (2024). https://doi.org/10.1039/D4TA03291H

[10] Md.A. Karim, K. Matsuishi, Md.E. Kayesh, Y. He, and A. Islam, "Inhibition of Sn^{2+} Oxidation in $FASnI_3$ Perovskite Precursor Solution and Enhanced Stability of Perovskite Solar Cells by Reductive Additive," ACS Appl. Mater. Interfaces. **15**, 45823-45833 (2023). https://doi.org/10.1021/acsami.3c07903

[11] Z. Chen, and T.P. Dhakal, "Room temperature synthesis of lead-free FASnI3 perovskite nanocrystals with improved stability by SnF_2 additive," Appl. Phys. Rev. **10**, (2023). https://doi.org/10.1063/5.0125100

[12] T. Wu, X. Liu, X. Luo, H. Segawa, G. Tong, Y. Zhang, L.K. Ono, *et al*., "Heterogeneous $FASnI_3$ Absorber with Enhanced Electric Field for High-Performance Lead-Free Perovskite Solar Cells," Nanomicro Lett. **14**, 99 (2022). https://doi.org/10.1007/s40820-022-00842-4

[13] S.Z. Haider, H. Anwar, and M. Wang, "A comprehensive device modelling of perovskite solar cell with inorganic copper iodide as hole transport material," Semicond. Sci. Technol. **33**, (2018). https://doi.org/10.1088/1361-6641/aaa596

[14] H. Sabbah, J. Arayro, and R. Mezher, "Numerical Simulation and Optimization of Highly Stable and Efficient Lead-Free Perovskite $FA_{1-x}Cs_xSnI_3$-Based Solar Cells Using SCAPS," Materials, **15**, 4761 (2022). https://doi.org/10.3390/ma15144761

[15] T.J. Macdonald, L. Lanzetta, X. Liang, D. Ding, and S.A. Haque, "Engineering Stable Lead-Free Tin Halide Perovskite Solar Cells: Lessons from Materials Chemistry," Advanced Materials, **35**, (2023). https://doi.org/10.1002/adma.202206684

[16] A. Tara, V. Bharti, S. Sharma, and R. Gupta, "Device simulation of $FASnI_3$ based perovskite solar cell with $Zn(O_{0.3}, S_{0.7})$ as electron transport layer using SCAPS-1D," Opt. Mater. (Amst). **119**, 111362 (2021). https://doi.org/10.1016/j.optmat.2021.111362

[17] S. Mattaparthi, D.K. Sinha, A. Bhura, and R. Khosla, "Design of an eco-friendly perovskite Au/NiO/FASnI3/ZnO0.25S0.75/FTO, device structure for solar cell applications using SCAPS-1D," Results in Optics, **12**, 100444 (2023). https://doi.org/10.1016/j.rio.2023.100444

[18] L. Nakka, Y. Cheng, A.G. Aberle, and F. Lin, "Analytical Review of Spiro-OMeTAD Hole Transport Materials: Paths Toward Stable and Efficient Perovskite Solar Cells," Advanced Energy and Sustainability Research, **3**, (2022). https://doi.org/10.1002/aesr.202200045

[19] S.N. Vijayaraghavan, K. Khawaja, J. Wall, W. Xiang, and F. Yan, "Photo-accelerated oxidation of spiro-OMeTAD for efficient carbon-based perovskite solar cells," Energy Advances, **3**, 1054–1061 (2024). https://doi.org/10.1039/D4YA00029C

[20] M.V. Kavitha, and K. Sudheer Sebastian, "Device modelling and performance enhancement of FASnI3-based perovskite solar cell with diverse, compatible charge transport layers," Results in Optics, **18**, 100783 (2025). https://doi.org/10.1016/j.rio.2025.100783

[21] T.M. Koh, T. Krishnamoorthy, N. Yantara, C. Shi, W.L. Leong, P.P. Boix, A.C. Grimsdale, *et al*., "Formamidinium tin-based perovskite with low Eg for photovoltaic applications," J. Mater. Chem. A Mater. **3**, 14996–15000 (2015). https://doi.org/10.1039/c5ta00190k

[22] M. Kumar, A. Raj, A. Kumar, and A. Anshul, "An optimized lead-free formamidinium Sn-based perovskite solar cell design for high power conversion efficiency by SCAPS simulation," Opt. Mater. (Amst). **108**, (2020). https://doi.org/10.1016/j.optmat.2020.110213

[23] A. Tara, V. Bharti, S. Sharma, and R. Gupta, "Device simulation of FASnI3 based perovskite solar cell with $Zn(O_{0.3}, S_{0.7})$ as electron transport layer using SCAPS-1D," Opt. Mater. (Amst). **119**, (2021). https://doi.org/10.1016/j.optmat.2021.111362

[24] L.K. Ono, S. (Frank) Liu, and Y. Qi, "Reducing Detrimental Defects for High-Performance Metal Halide Perovskite Solar Cells," Angewandte Chemie International Edition, **59**, 6676–6698 (2020). https://doi.org/10.1002/anie.201905521

[25] J. Siekmann, S. Ravishankar, and T. Kirchartz, "Apparent Defect Densities in Halide Perovskite Thin Films and Single Crystals," ACS Energy Lett. **6**, 3244–3251 (2021). https://doi.org/10.1021/acsenergylett.1c01449

[26] M.K. Hossain, G.F.I. Toki, A. Kuddus, M.K.A. Mohammed, R. Pandey, J. Madan, S. Bhattarai, *et al*., "Optimization of the architecture of lead-free CsSnCl3-perovskite solar cells for enhancement of efficiency: A combination of SCAPS-1D and wxAMPS study," Mater. Chem. Phys. **308**, 128281 (2023). https://doi.org/10.1016/j.matchemphys.2023.128281

[27] E. Danladi, A.C. Egbugha, R.C. Obasi, N.N. Tasie, C.U. Achem, I.S. Haruna, and L.O. Ezeh, "Defect and doping concentration study with series and shunt resistance influence on graphene modified perovskite solar cell: A numerical investigation in SCAPS-1D framework," Journal of the Indian Chemical Society, **100**, 101001 (2023). https://doi.org/10.1016/j.jics.2023.101001

[28] Kavitha M.V., S. Sebastian K., "A numerical study to enhance the performance of $FASnI_3$ -based HTL-free inverted perovskite solar cell with compatible electron transport layers," Phys. Scr. **100**, 075931 (2025). https://doi.org/10.1088/1402-4896/addf1a

[29] M.K. Hossain, M.H.K. Rubel, G.F.I. Toki, I. Alam, Md.F. Rahman, and H. Bencherif, "Effect of Various Electron and Hole Transport Layers on the Performance of $CsPbI_3$ -Based Perovskite Solar Cells: A Numerical Investigation in DFT, SCAPS-1D, and wxAMPS Frameworks," ACS Omega, **7**, 43210–43230 (2022). https://doi.org/10.1021/acsomega.2c05912

[30] A. Ahmed, K. Riaz, H. Mehmood, T. Tauqeer, and Z. Ahmad, "Performance optimization of $CH3NH3Pb(I_{1-x}Br_x)_3$ based perovskite solar cells by comparing different ETL materials through conduction band offset engineering," Opt. Mater. (Amst). **105**, 109897 (2020). https://doi.org/10.1016/j.optmat.2020.109897

[31] K. Hongsith, V. Yarangsi, S. Sucharitakul, S. Phadungdhitidhada, A. Ngamjarurojana, and S. Choopun, "A Multi-Electron Transporting Layer for Efficient Perovskite Solar Cells," Coatings, **11**, 1020 (2021). https://doi.org/10.3390/coatings11091020

[32] A.K. Singh, R. Walia, M.S. Chauhan, R.S. Singh, and V.K. Singh, "Performance analysis of n-TiO_2/p-Cu_2O, n-TiO_2/p-WS_2/p-Cu_2O, and n-TiO_2/p-WS_2 heterojunction solar cells through numerical modelling," Environmental Science and Pollution Research, **30**, 98718–98731 (2022). https://doi.org/10.1007/s11356-022-24236-6

[33] A.S. Yusuf, A.M. Ramalan, A.A. Abubakar, and I.K. Mohammed, "Effect of Electron Transport Layers, Interface Defect Density and Working Temperature on Perovskite Solar Cells Using SCAPS 1-D Software," East European Journal of Physics, (1), 332-341 (2024). https://doi.org/10.26565/2312-4334-2024-1-31

[34] K.S. Nithya, and K.S. Sudheer, "Numerical modelling of non-fullerene organic solar cell with high dielectric constant ITIC-OE acceptor," J. Phys. Commun. **4**, 025012 (2020). https://doi.org/10.1088/2399-6528/ab772a

[35] Y. Gan, X. Bi, Y. Liu, B. Qin, Q. Li, Q. Jiang, and P. Mo, "Numerical Investigation Energy Conversion Performance of Tin-Based Perovskite Solar Cells Using Cell Capacitance Simulator," Energies, (Basel), **13**, 5907 (2020). https://doi.org/10.3390/en13225907

ЧИСЛОВЕ МОДЕЛЮВАННЯ ДОСЛІДЖЕННЯ ФУНКЦІОНАЛЬНОСТІ ПЕРОВСКІТНОГО СОНЯЧНОГО ЕЛЕМЕНТА НА ОСНОВІ FASnI3 У ЗВИЧАЙНІЙ, ТА ІНВЕРТОВАНІЙ КОНФІГУРАЦІЯХ З ВИКОРИСТАННЯМ СУМІСНОГО $Zn(O_{0.3}S_{0.7})$ ЯК ШАРУ ЕЛЕКТРОННОГО ТРАНСПОРТУ

М.В. Кавіта[1,2], К.С. Судхір[1,3]

[1]Дослідницька лабораторія моделювання оптоелектронних пристроїв, кафедра фізики, Коледж Христа (автономний), Іринджалакуда, Калікутський університет, Керала, Індія, PIN-680125

[2]Кафедра фізики, Коледж Шрі Нараяна, Наттіка, Калікутський університет, Керала, Індія, PIN-680566

[3]Кафедра фізики, Коледж Святого Алоїзія, Тріссур, Калікутський університет, Керала, Індія, PIN-680611

Йодид формамідинію олова є перспективним кандидатом на роль поглинального шару в перовскітних сонячних елементах завдяки регульованій ширині забороненої зони, високому коефіцієнту поглинання та добрій термічній стабільності. Вибір відповідних шарів переносу заряду з належним зміщенням зони може ефективно зменшити рекомбінацію на межі розділу та підвищити продуктивність сонячного елемента. Дослідження зосереджено на підвищенні продуктивності перовскітного сонячного елемента, в якому йодид формамідинію олова ($FASnI_3$) є поглинальним шаром, $Zn(O_{0.3}S_{0.7})$ - ETL, a Spiro-OMeTAD - HTL, за допомогою числового моделювання. Ці матеріали шару переносу заряду вибрані на основі їх адекватного вирівнювання енергетичної зони з поглиначем. Структура скляна підложка/FTO/$Zn(O_{0.3}S_{0.7})$(ETL)/$FASnI_3$/Spiro-OMeTAD(HTL)/Au, яка є недослідженою комбінацією в n-i-p архітектурі, була змодельована за допомогою SCAPS-1D, та проведена оптимізація параметрів комірки – товщини поглинача, концентрації легування поглинача, щільності дефектів поглинача, товщини ETL, щільності дефектів ETL, товщини HTL та щільності дефектів HTL. Також проаналізовано зміну параметрів роботи комірки залежно від щільності дефектів на межі розділу та температури. Завдяки цій оптимізації комірка забезпечує напругу холостого ходу (Voc) = 1,0145 В, щільність струму короткого замикання (Jsc) = 37,82 мА $см^{-2}$, коефіцієнт заповнення (FF) = 83,31% та коефіцієнт перетворення енергії (PCE) = 31,97%. Оптимізовані параметри використовуються для моделювання інвертованої p-i-n архітектури, а вихідна напруга *елемента така: Voc = 1,0919 В, Jsc = 37,293 мА $см^{-2}$, FF = 83,01% та ККД перетворення енергії (PCE) = 33,8%.*

Ключові слова: *перовскітний сонячний елемент; SCAPS; формамідиній-олов'яний йодид; спіро-OMeTAD, ZnOS*